

Koponen, S., Attila, J., Pulliainen, J., Kallio, K., Pyh alahti, T., Lindfors, A., Rasmus, K., and Hallikainen, M., A case study of airborne and satellite remote sensing of a spring bloom event in the Gulf of Finland. *Continental Shelf Research*, in press, 2006.

  2006 by authors and   2006 Elsevier Science

Preprinted with permission from Elsevier.

A Case Study of Airborne and Satellite Remote Sensing of a Spring Bloom Event in the Gulf of Finland

Sampsa Koponen^{*1}, Jenni Attila², Jouni Pulliainen¹, Kari Kallio², Timo Pyh lahti², Antti Lindfors³, Kai Rasmus⁴, Martti Hallikainen¹

*Corresponding author

1. Laboratory of Space Technology, Helsinki University of Technology

PO BOX 3000, 02015 HUT, FINLAND

Tel. +358 9 4512374, fax. +358 9 4512898

Email: sampsa.koponen@hut.fi

2. Finnish Environment Institute, PO BOX 140, SF-00251 Helsinki, FINLAND

3. Luode Consulting OY, Olarinluoma 15, FI-02200 Espoo, FINLAND

4. Division of Geophysics, University of Helsinki, PL 64, 00014 University of Helsinki, FINLAND

ABSTRACT

The concentrations of chlorophyll-*a* (chl *a*), total suspended solids (TSS) and the absorption coefficient of colored dissolved organic matter ($a_{CDOM(400)}$) are estimated in Case II waters using MERIS satellite (FR level 1b, 300 m resolution) and AISA airborne spectrometer data acquired during a spring bloom in the Gulf of Finland, Baltic Sea on April 27, 2004. The accuracy of the estimation is analyzed using empirical band-ratio algorithms together with *in situ* observations that include water samples analyzed in a laboratory (variation ranges: 22-130 $\mu\text{g/l}$, 2.9-20 mg/l , and 1.29-2.61 m^{-1} for chl *a*, TSS and $a_{CDOM(400)}$, respectively). Additional *in situ* estimates (transects) on these characteristics are available through absorption and scattering coefficients measured with an ac-9 absorption and attenuation meter installed in a flow-through system. The retrieval accuracy (R^2) of all three water quality characteristics with MERIS data is close to or above 0.9, while the RMSE is 7.8 $\mu\text{g/l}$ (22 %), 0.74 mg/l (16 %) and 0.08 m^{-1} (5 %), for chl *a*, TSS and $a_{CDOM(400)}$, respectively. The validity of the chl *a* algorithm is tested using nine additional data points. The BIAS-error for these points is 5.2 $\mu\text{g/l}$ and the RMSE is 10.6 $\mu\text{g/l}$. The effects of changes in the atmospheric characteristics on band-ratio algorithms in cases where no concurrent *in situ* reference data are available are analyzed using the MODerate spectral resolution atmospheric TRANSmittance algorithm and computer model (MODTRAN). The additional error due to these changes is estimated to be below 20 % for the applied ratio algorithms. The water quality data available in the level 2 MERIS-product distributed by the European Space Agency did not include valid results for the date investigated here.

Keywords: MERIS, flow-through ac-9, chlorophyll-*a*, colored dissolved organic matter, total suspended solids, Baltic Sea, Gulf of Finland

1 INTRODUCTION

Natural water found in rivers, lakes and oceans is a mixture of water and a variety of organic and inorganic substances. Some of these interact with visible light and are hence called optically significant substances (OSS). The following three are commonly identified as the most important OSS:

1. **Chlorophyll-a** (chl *a*) is a pigment that is present in phytoplankton cells and its concentration is a proxy measurement of phytoplankton biomass.
2. **Total Suspended Solids** (TSS) include the organic and inorganic particles suspended in water (e.g. clay particles; phytoplankton).
3. **Colored Dissolved Organic Matter** (CDOM, also known as yellow substances, humic matter or gelbstoff) includes compounds produced during the decay of plant matter.

Each substance has its own wavelength-dependent absorption, scattering and back-scattering coefficients $a(\lambda)$, $b(\lambda)$ and $b_b(\lambda)$, respectively. These coefficients, together with the absorption, scattering and backscattering coefficients of pure water, determine how solar radiation interacts with water. Hence, by analyzing the spectra emanating from water, it is possible to estimate the type and the amount of OSS found in it. This is the basis of the remote sensing of water quality.

Areas where the most important OSS is chl *a* and the substances that co-vary with it are defined as Case I waters (Morel and Prieur, 1977). These usually include oceanic areas. In Case II waters (most coastal areas and lakes) the values of OSS can be much larger than in oceans and they can also vary independently from each other. This makes the remote sensing of water quality in Case II waters more difficult. Typical values of OSS and their influence on the detected radiance in the Baltic Sea have been presented recently for example in Darecki and Stramski (2004), Siegel et al. (2005) and Kowalczyk et al. (2005).

The Finnish coast (part of the Baltic Sea) is quite fragmented. It contains numerous small islands, peninsulas and bays which complicate the use of remote sensing for water quality estimation. Therefore, one of the main characteristics of a remote sensing instrument intended for monitoring the quality of coastal water is its spatial resolution. Proper channel combination with sufficient spectral resolution, frequent overpasses and good availability of data are the other important factors.

The Medium Resolution Imaging Spectrometer (MERIS) onboard the Envisat satellite (Rast et al. 1999) has 300 m resolution (FR, or Full Resolution, data are used here) and 15 channels in the visible to near-infrared (NIR) region (from 412.5 to 900 nm). Hence, it is an ideal candidate for monitoring fragmentary coastal regions such as the coastline of Finland.

The objective of this paper is to investigate the feasibility of MERIS for estimating the values of the three main OSS during a spring bloom event in the Gulf of Finland. In addition to satellite data, we use data from an airborne imaging spectrometer AISA (Airborne Imaging Spectrometer for Applications; Specim, 2005) that has a substantially larger band selection and a better spatial resolution than MERIS.

The retrieval accuracy is analyzed using empirical band-ratio algorithms together with an extensive set of *in situ* observations. Earlier studies using AISA (Härmä et al. 2001;

Kallio *et al.* 2003; Koponen *et al.* 2001), simulated MERIS data (Koponen *et al.* 2002), real MERIS data (Ruddick *et al.* 2004), and other instruments (Dekker 1993; Gitelson *et al.* 1993, Ruddick *et al.* 2001) have shown that algorithms based on ratios of two bands (NIR/red) yield good results for chl *a* in Case II waters. Simulations of water-leaving radiance reflectances of three lakes in Sweden by Pierson and Strömbeck (2000) show that an algorithm suitable for CDOM estimation is a ratio of a channel with wavelength > 600 nm to a channel with wavelength in the 400-580 nm range. Kallio *et al.* (2005) used spectrometer data measured from a boat to confirm this by obtaining good correlations for CDOM with channel ratio $R_{662-672}/R_{483-493}$.

In contrast to the color indices used in this work the level 2 MERIS product distributed by the European Space Agency (ESA) is based on the use of neural networks (NN). This inherently different method is presented by Schiller and Doerffer (1999). The input for the NN includes atmospherically corrected reflectances of eight MERIS channels. MERIS potential for monitoring coastal CASE II waters has been investigated earlier for example in Doerffer *et al.* (1999).

The amounts of aerosols (dust, haze, etc.) and gases (ozone, water vapor, etc.) present in the atmosphere vary both spatially and temporally. These variations can disturb the estimation of water quality characteristics when remote sensing methods are used. Even though band-ratio algorithms reduce the effect of these disturbances, the atmosphere often remains as the most important source of error in the remote sensing of water quality. Since in this study we investigate empirical algorithms with concurrent *in situ* observations, atmospheric correction is not relevant for the data analysis as the effects of the atmospheric parameters on the water quality estimation are already included in the coefficients of the algorithms. However, when data from different dates and locations are compared an atmospheric correction is necessary, especially if *in situ* observations to calibrate the algorithms are not available. Unfortunately, atmospheric correction methods often fail in the coastal areas of the Baltic Sea because the assumptions made during the correction about the amount of OSS in water are not valid. For example, the atmospheric correction methods developed for oceanic waters fail in coastal regions since the assumption about the water-leaving radiance in the infrared being zero is not valid. Also, in the Baltic Sea the high amount of CDOM causes problems for the atmospheric correction of MERIS data (Brockmann *et al.*, 2002). In addition, the sun elevation angle is relatively low in the high latitudes of the Nordic region.

In this investigation the effects of atmospheric variations on the retrieval performance of the band-ratio algorithms are analyzed using lookup tables of atmospheric transmittance and radiance. These characteristics are simulated with the MODerate spectral resolution atmospheric TRANSmittance algorithm and computer model (MODTRAN) (Berk *et al.*, 1989). The results indicate the magnitude of the retrieval error when an empirical band-ratio algorithm developed under certain atmospheric conditions is used for other occasions or regions without reference *in situ* data for calibrating the algorithm. The atmosphere over Baltic Sea generally is clear according to the aerosol optical thickness (AOT) measurements from the Aerosol Robotic Network (AERONET) near the island of Gotland (Carlund *et al.*, 2005). According to Carlund *et al.* (2005), daily median value of the optical depth at 500 nm was about 0.08. During the measurement day, the average measured AOT (at 500 nm) was 0.12 on Toravere, Estonia.

2 METHODS

2.1 Data

The data used in this study were collected during a multi-sensor water quality measurement campaign conducted at the coast of Finland, near the city of Helsinki on April 27, 2004. The campaign took place during an algae spring bloom dominated by dinoflagellates and diatoms. The spatial variations of OSS were substantial within the measurement area. In addition to the extensive *in situ* observations, the dataset includes airborne and spaceborne remote sensing observations.

The weather was clear during the campaign. There was no cloud cover over the measurement area at the time of the boat and airborne measurements. However, clouds started to form near the coast after the airborne campaign and affected the spaceborne data in the northernmost part of the measurement area.

The measurement area is shown in Figure 1. Water depth in the area varies from 5 m near the coast to about 40 in the open sea. There are no rivers near the campaign area. However, there is a harbor construction site about 500 m from station 1 which can affect the water quality in the area.

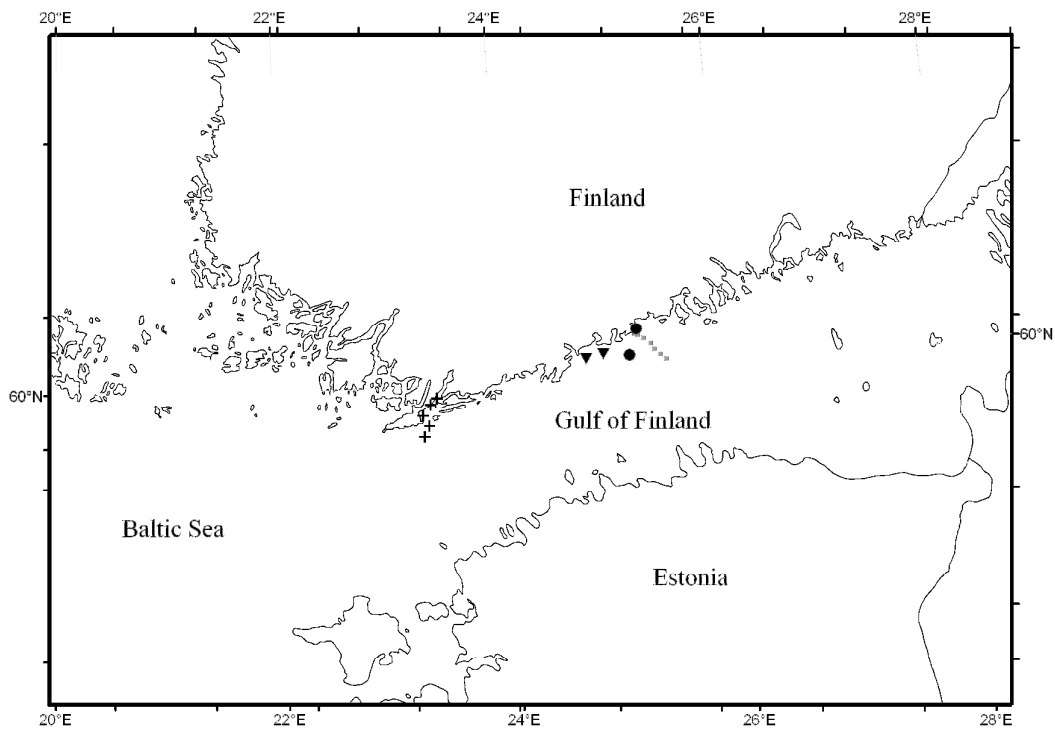


Figure 1. Map of the campaign area. The location of the measurement transect is shown as small grey squares (■). The locations of validation data 1, 2 and 3 are marked with ▼, ● and +, respectively.

The area has ice cover during most winters. When the ice melts in the early spring the amount of solar radiation in water increases and biological activity starts to grow, which leads to a phytoplankton spring bloom. The concentration of chl *a* in a spring bloom can be over 200 $\mu\text{g/l}$. The phytoplankton cells are mixed in the upper layer of water, from surface to a depth of a few meters (i.e. not like cyanobacteria, which is often floating on the surface).

2.1.1 *In situ* observations

The *in situ* observations include a 28 km long transect measured with a flow-through measurement system (Lindfors et al. 2005) installed on a boat (measurement depth 0.5 m; 5103 data points), water samples collected at ten fixed stations (S1-S10) along the transect (measurement depth 0.5 m), and five Secchi depth (SD) measurements. The data were collected between 10:30 and 11:46 a.m. local time (GMT+3). The samples were analyzed in a laboratory and yielded concentrations for chl *a* and TSS, and the absorption coefficient of CDOM at 400 nm ($a_{\text{CDOM}(400)}$). The values of the laboratory measurements are shown in Table 1. The sum of chlorophyll *a* and phaeophytin *a* (denoted here with chl *a*) was determined with a spectrophotometer after extraction with hot ethanol (ISO 10260). TSS was determined with the gravimetric method using a GF/F filter (EN 872). $a_{\text{CDOM}(400)}$ was measured with a spectrophotometer (50 mm long cuvette) from a sample filtered through a GF/F filter.

The boat transect started near the coast and extended towards the open sea between a few islands. As can be seen in Table 1 the values of the OSS have large ranges of variation. The values also decrease as the distance from the shore increases. However, the decrease is not always monotonous. For example, the value of the chl-*a* concentration has a sudden decrease at station S5. It then increases at S6 and starts to decrease again.

The flow-through system measures temperature, conductivity, and total absorption and scattering coefficients ($a_{\text{tot}}(\lambda)$ and $b_{\text{tot}}(\lambda)$, respectively) at 9 wavelengths (λ , between 412 and 715 nm) using the WET Labs ac-9 absorption and attenuation meter.

Table 1. Results of the laboratory analyzes and Secchi depth at the fixed stations.

Station number	Chl <i>a</i> ($\mu\text{g/l}$)	TSS (mg/l)	$a_{\text{CDOM}(400)}$ (m^{-1})	Secchi Depth (m)	Latitude WGS84	Longitude WGS84
S1	110	20	2.61	0.6	60°12.80'	25°11.71'
S2	100	16	2.44	-	60°12.30'	25°11.60'
S3	130	18	2.42	0.6	60°11.68'	25°11.48'
S4	95	12	2.15	-	60°10.49'	25°10.55'
S5	22	5.2	2.01	1.4	60°10.07'	25°12.26'
S6	65	7.7	1.55	-	60°09.17'	25°15.30'
S7	42	4.4	1.32	2.8	60°07.63'	25°18.93'
S8	40	4.4	1.31	-	60°06.10'	25°20.66'
S9	22	3.4	1.30	3.5	60°04.59'	25°23.66'
S10	22	2.9	1.29	-	60°03.23'	25°26.54'

2.1.2 Airborne data

The AISA-instrument used in the airborne part of the campaign was flown along the boat transect at 1 km altitude onboard a Short SC-7 Skyvan research aircraft. The data were collected between 11:34 and 11:55 a.m. local time (GMT+3). AISA data cover nine of the ten *in situ* stations. Although AISA has 286 channels it can use only a fraction of those in the imaging mode suitable for airborne remote sensing. For this campaign 32 channels that match the MODIS (EOS Terra and Aqua satellites) and MERIS channels in the wavelength range 437-891 nm were selected. The AISA measurement system includes a GPS receiver and an inertial navigation system, which allow the data to be geolocated automatically. After geolocation the pixel size is 2 by 2 m.

AISA is calibrated using calibration lamps. According to the manufacturer the error of the radiance measurement is 5-10% (the error is of the 'bias type' which means it tends to be biased, i.e. the whole measured spectrum is either above or below the correct one and the shape of the measured spectrum closely matches the correct one).

2.1.3 Spaceborne data

The spaceborne data include FR level 1b (calibrated top of the atmosphere (TOA) radiances) MERIS observations acquired within two hours from the start of the *in situ* observations (acquisition time 12:35 local time). The sensor zenith angle θ_{sat} for the measurement area was 18° , while the solar zenith angle θ_{sun} was 47° .

A level 2 (FR__2P, 300 m resolution, geophysical data) product of the same date and time was also obtained from ESA (Processing time of data: 16 March 2005; software version: MERIS/4.10). The product contains the concentrations of phytoplankton (algal_2) and suspended sediments (total_susp), and the absorption coefficient of yellow substances at 440 nm (yellow_subs).

2.2 ANALYSIS

2.2.1 Airborne data

The AISA radiances (L_{AISA}) at the sampling stations were extracted by finding the AISA pixel closest to the location of each station. The average radiance values within an 11 by 11 pixel area around each station were also extracted. The averaging was performed in order to reduce the small scale variability in the AISA data caused by waves and instrument noise. The same procedure was then used with the flow-through data points. As the AISA data does not cover the whole boat transect, the number of usable data points for the analysis with combined AISA and flow-through data is 4649.

The AISA instrument also includes a sensor for measuring the downwelling irradiance (E_d) that can be used for transforming the measured radiance into an estimate of the remote sensing reflectance ($R_{\text{RS}} = L_{\text{AISA}}/E_d$) at the altitude of the aircraft. These reflectance values are shown in Figure 2. However, since the use of E_d in the computation adds uncertainty to the analysis of the airborne data the analysis is conducted with radiance values. The radiance data are not atmospherically corrected. The sky light reflected by the water surface (air-water interface) has not been removed.

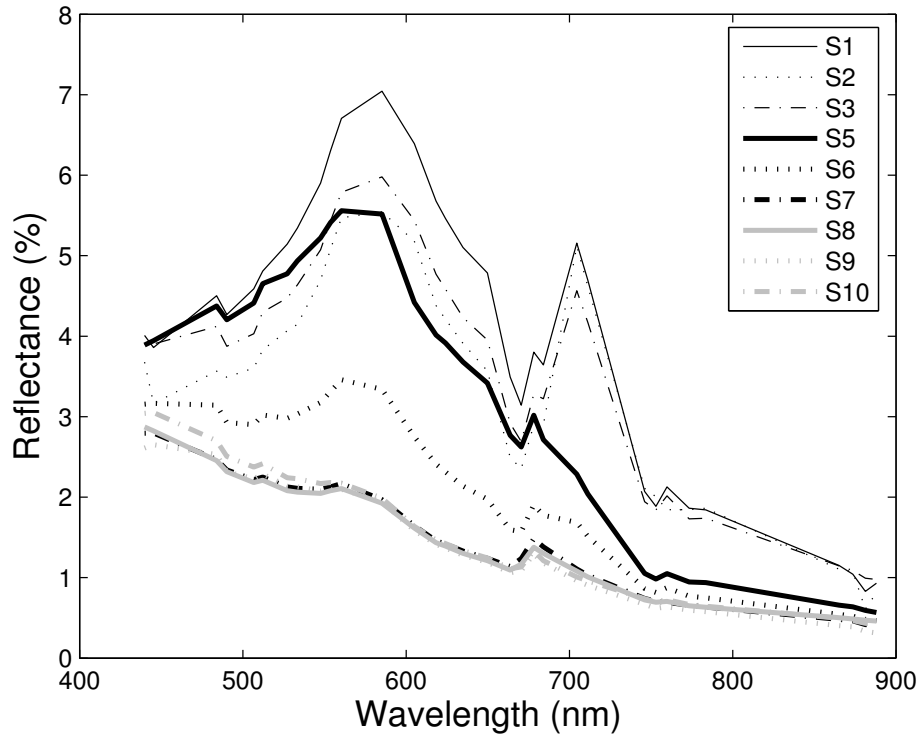


Figure 2. Uncorrected AISA reflectances observed over the water sample collection stations at a flight altitude of 1 km.

The channel combinations for the algorithms of each OSS are based on the results from previous studies (Härmä *et al.* 2001; Kallio *et al.* 2003; Koponen *et al.* 2001; Koponen *et al.* 2002). The algorithms for chl *a* and $a_{CDOM}(400)$ are composed of band ratios while for TSS a single channel is used.

2.2.2 Spaceborne data

The MERIS radiances at the sampling stations were extracted by finding the closest MERIS pixel after geolocation. Cloud cover prevented the observation of sampling stations S1, S2 and S3 with MERIS. Hence, those three data points were excluded from the satellite data analysis.

For the flow-through data the extraction was performed by finding the flow-through values located within each MERIS pixel and averaging them. The number of these data points was 73 after cloudy pixels were removed.

The analysis of the MERIS data was similar to the one performed with airborne data. The biggest difference is that now the algorithm for TSS is also based on a band-ratio since the R^2 value for the single channel algorithm was less than 0.8.

The root mean square error (RMSE) of a linear regression can be derived with equation:

$$\text{RMSE} = \sqrt{\frac{1}{N-2} \sum_{i=1}^N (OSS_{FT,i} - OSS_{MERIS,i})^2} \quad (1)$$

where N , OSS_{FT} and OSS_{MERIS} are the number of data points, the values of flow-through data and the values derived with MERIS data, respectively.

2.2.3 Effects of atmospheric variations on MERIS estimation

The algorithms presented here are empirical in nature, and hence valid only for the atmospheric (and other) conditions that prevailed during the campaign. While one-time retrieval results such as the ones presented here are valuable to end-users of water quality data, one of the main goals of remote sensing is to produce reliable time series of water quality maps. In order to estimate the accuracy of using the algorithms developed here with satellite data acquired on different dates (and hence different atmospheric conditions), and without additional *in situ* observations, the procedure outlined below was performed. The procedure is not intended to be a method for atmospheric correction per se, but as a tool for estimating the likely error caused by the atmosphere.

First the two-way atmospheric transmittance (from the top of the atmosphere down to the surface and back to the top of the atmosphere), $T_{atm}(\lambda, \theta_{sat})$ and the atmospheric radiance, $L_{atm}(\lambda, \theta_{sun}, \theta_{sat})$, at MERIS channels are computed for three cases. These represent the situations where the atmospheric visibilities are 25, 35 and 40 km. The atmospheric model used in the simulations is *Subarctic Summer* and the aerosol type was a combination of rural, maritime and urban. The simulated values are shown in Table 2. The values for visibility were selected according to statistics calculated from the weather stations of the Finnish Meteorological Institute. The visibility ranges from 25 to 40 km on a typical summer day between 9 and 12 a.m. at the coastal weather stations. The closest weather station of Finnish Meteorological Institute observed visibility values ranging from 25 km to 35 km during the day of the *in situ* measurements. During the morning (9-12 a.m. local time), the visibility was 35 km. During the afternoon (3 p.m. local time), the visibility was lower, 25 km.

Table 2. Atmospheric parameters simulated with MODTRAN for visibility values of 25, 35 and 40 km. Atmospheric model: Subarctic Summer. Aerosol type: a combination of rural, maritime and urban.

Channel wavelength (nm)	Total atmospheric transmittance, T_{atm}			Atmospheric radiance, L_{atm} ($W m^{-2} sr^{-1} \mu m^{-1}$)		
	25 km	35 km	40 km	25 km	35 km	40 km
412.5	0.472	0.530	0.544	71.5	63.0	61.4
442.5	0.526	0.586	0.601	64.4	55.5	53.7
490 ^a	0.595	0.654	0.671	49.5	41.6	39.7
510	0.616	0.674	0.692	43.4	36.1	34.3
560 ^a	0.660	0.714	0.732	29.8	24.3	22.7
620	0.703	0.753	0.772	20.6	16.3	15.1
665 ^a	0.743	0.791	0.809	16.1	12.6	11.5
681.25	0.757	0.804	0.822	14.7	11.4	10.4
708.75 ^a	0.756	0.801	0.824	12.5	9.7	8.9

^a Channels used in the estimation of OSS.

The visibility can of course have much smaller values. However, in those cases the cloud cover, humidity and other factors that limit the visibility are likely to prevent remote sensing observations altogether. Hence, we consider here only the range of visibility where the use of satellite images is still likely to be successful.

Next the observed MERIS TOA radiances, $L_{TOA}(\lambda, \theta_{sun}, \theta_{sat})$, are all assumed to belong to the 35 km –case and the normalized (i.e. before it enters the atmosphere) radiances in space, $L_{TOA}^*(\lambda, \theta_{sun}, \theta_{sat})$, are computed with equation

$$L_{TOA}^* = \frac{L_{TOA} - L_{atm, 35 km}}{T_{atm, 35 km}}. \quad (2)$$

Then the MERIS TOA radiances that would be observed with the 25 and 40 km –cases, $L_{25km}(\lambda, \theta_{sun}, \theta_{sat})$ and $L_{40km}(\lambda, \theta_{sun}, \theta_{sat})$, are computed with

$$L_{TOA, 40km} = L_{TOA}^* T_{atm, 40 km} + L_{atm, 40 km}, \quad (3)$$

and

$$L_{TOA, 25km} = L_{TOA}^* T_{atm, 25 km} + L_{atm, 25 km}. \quad (4)$$

Next, $L_{TOA, 40 km}$ and $L_{TOA, 25 km}$ are used in the retrieval of chl a , $a_{CDOM(400)}$ and TSS using algorithms derived with the original data. Finally, the relative errors (RE) in comparison to the original data are computed with

$$RE = \frac{chl a_{40km} - chl a_{35km}}{chl a_{35km}}. \quad (5)$$

For the other cases and variables the error is computed using the same method.

3 RESULTS

3.1 *In situ* data

Based on the results from the laboratory analysis it is possible to develop algorithms (Figure 3) that transform $b_{tot}(\lambda)$ and $a_{tot}(\lambda)$ measured with ac-9 into OSS values. This yields 5103 data points with full OSS information, which with airborne and spaceborne remote sensing data can be used for testing and further development of retrieval algorithms. The correlations between the *in situ* OSS are shown in Table 3.

3.2 Airborne data

The channel combinations and the regression coefficients with the present airborne dataset and the OSS values collected at the sampling stations are shown in Figure 4 along with the corresponding scatter plots. All data points are close to the trend line except station S2 for chl a . Visual examination (not shown here) of AISA data shows that the water surrounding S2 has a very strong spectral peak near 700 nm (corresponding chl a concentrations according to our AISA-algorithm are near 200 $\mu\text{g/l}$). The westernmost edge of this area is approximately 50 m from S2 while in the east the area extends beyond the AISA image. Wind direction was from east (80° from N) during the campaign so the area is likely to be a strong bloom that has drifted into

the transect after the measurement boat has passed. Hence, the most likely reason why S2 is an outlier for chl *a* is water transport. The chl *a* data from S2 were excluded from the analysis when the coefficients for the algorithms presented in Figure 4 were computed.

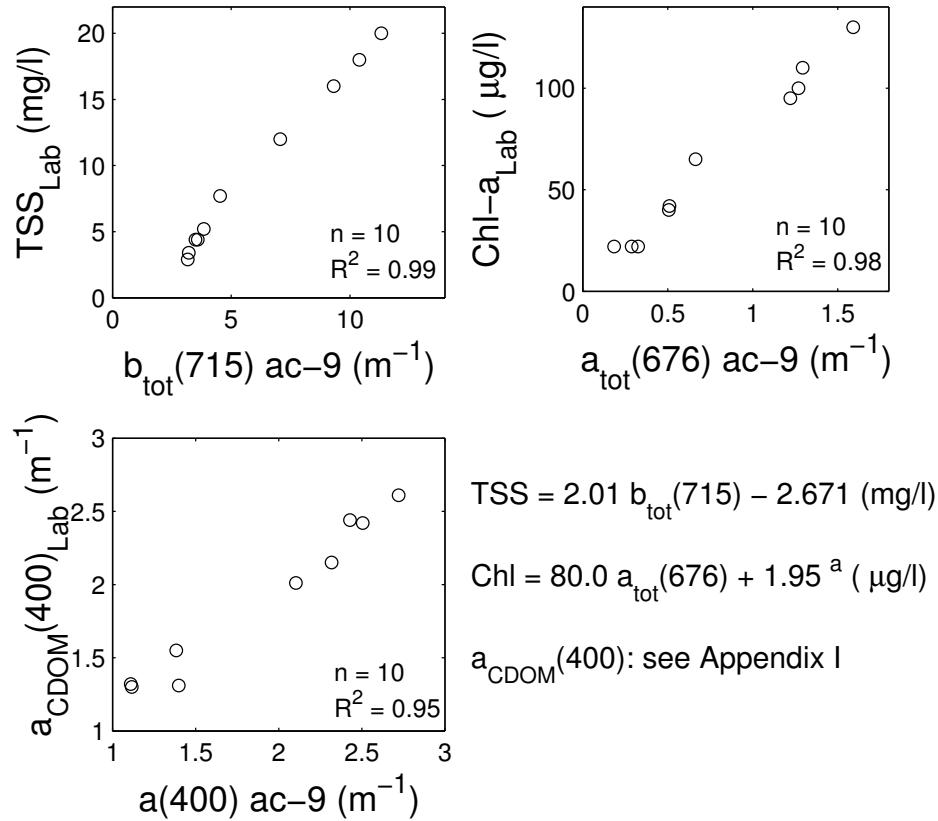


Figure 3. Correlations between OSS measured in laboratory (Lab) and the ac-9 measurements at ten stations. 'a(400) ac-9' is the absorption coefficient of CDOM estimated from the ac-9 data. See Appendix I for details. n is the number of data points and R^2 is the coefficient of determination. ^a In the chl *a* algorithm, the absorption of pure water has been subtracted. Absorption by CDOM and detritus in the red region are assumed negligible.

Table 3. The correlations coefficients (r) between chl *a*, $a_{CDOM(400)}$ and TSS with water sample and flow-through data.

	Chl <i>a</i> & TSS	Chl <i>a</i> & $a_{CDOM(400)}$	$a_{CDOM(400)}$ & TSS	n
Water sample	0.96	0.84	0.93	10
Flow-through	0.95	0.75	0.85	5103

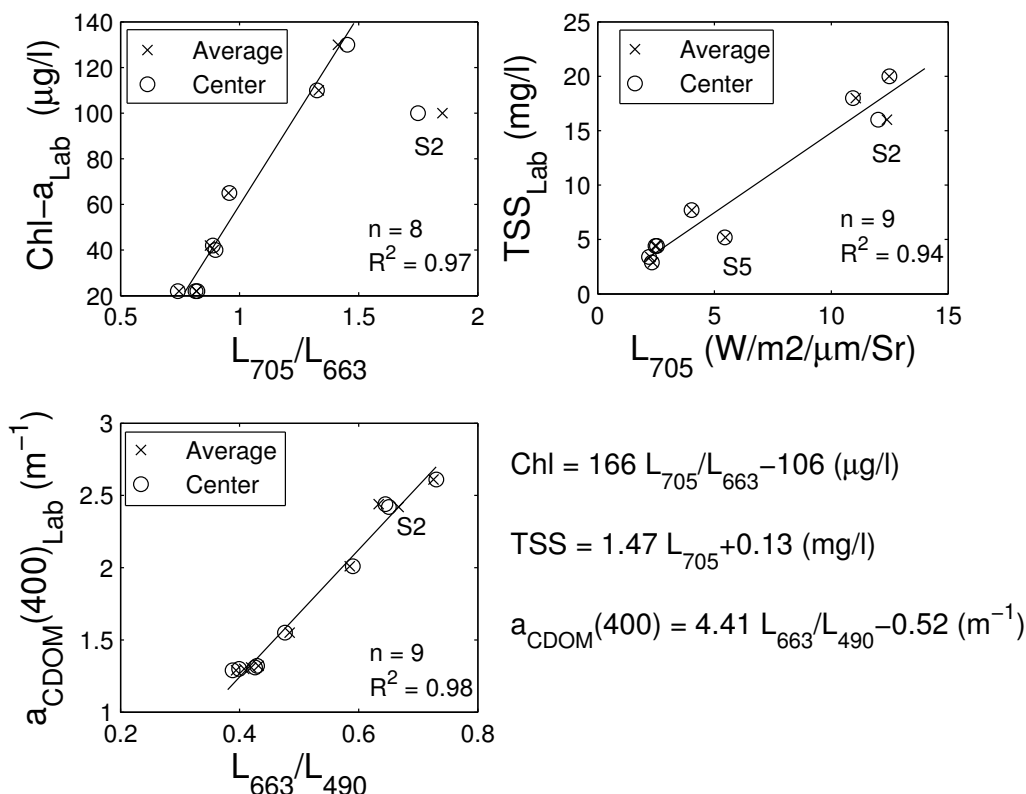


Figure 4. The correlations between AISA algorithms and OSS measured in laboratory. ‘Average’ values are the mean radiance of pixels within an 11*11-pixel window centered on the sampling station. ‘Center’ values are the radiance values of the pixels closest to the station. S2 is an outlier for chl a and it is excluded from this analysis. n is the number of data points used for deriving the algorithms. R^2 is the coefficient of determination. If station S2 is excluded from the TSS analysis the R^2 value improves to 0.95.

The airborne data also show that Chl a and TSS concentrations can have very dynamic spatial features. The values of $a_{\text{CDOM}}(400)$ in turn change much more steadily as a function of distance (from the beginning of the transect) and seem not to be as susceptible to local changes as chl a and TSS are. With MERIS data the problem of water transport is not as serious because of larger pixel size.

The AISA radiances were compared with the flow-through data using the same channels as used with the laboratory samples. The resulting R^2 values are shown in Table 4, while Figure 5 shows scatter plots for chl a and $a_{\text{CDOM}}(400)$. The data points around S2 are again outliers for chl a . If those are excluded from the analysis R^2 improves from 84.1 to 94.1. For $a_{\text{CDOM}}(400)$ the data points around S2 are not outliers. When the data is filtered by applying a moving average filter (the value of each data point is replaced with the average of the neighboring data points within a span that is 40 samples long) the results improve, especially for $a_{\text{CDOM}}(400)$. These values are also shown in Table 4.

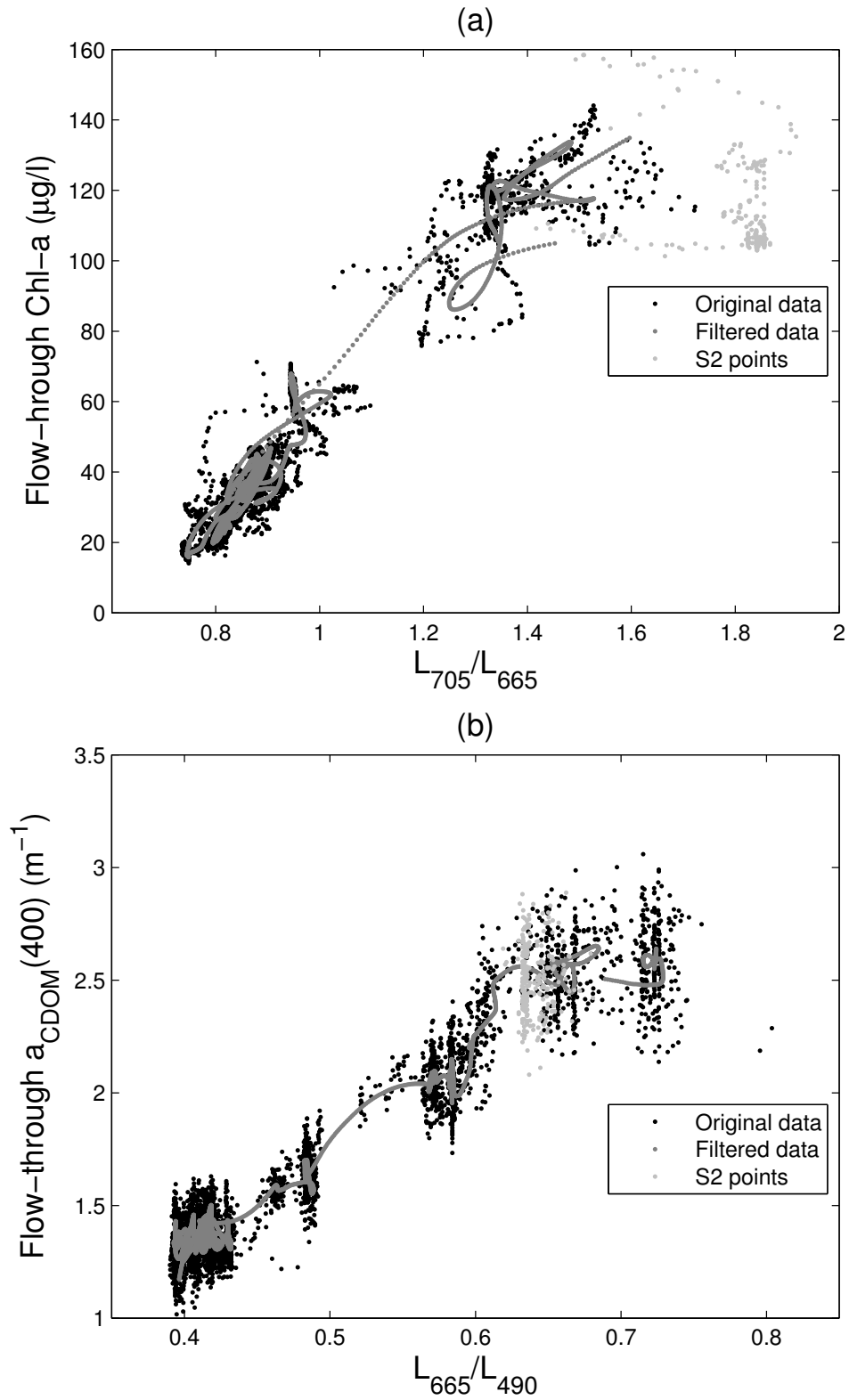


Figure 5. AISA data vs. flow-through values for (a) chl *a* and (b) $a_{\text{CDOM}}(400)$.

Table 4. Retrieval algorithms and the coefficients of determination (R^2 in %) for AISA and flow-through data in different cases.

	Chl a ($\mu\text{g/l}$)	TSS (mg/l)	$a_{\text{CDOM}}(400)$ (m^{-1})
Algorithm	$160 \frac{L_{705}}{L_{663}} - 103$	$1.49 L_{705} - 0.16$	$4.40 \frac{L_{663}}{L_{490}} - 0.45$
All data (n = 4649)	84.1	93.7	92.5
After filtering	86.1	94.2	97.1
Without S2 data (n = 4408)	94.1	93.0	92.5

Figure 6 shows the values of each OSS retrieved with AISA and flow-through data as a function of the distance from the beginning of the boat transect after the data have been filtered. The remote sensing data agree with the *in situ* observations quite well. Only in a few locations (S2 for chl a ; and S5 for TSS) the curves do not follow each other. Figure 6 also shows in more detail that the values of the OSS do not always follow each other. Especially chl a has large and sudden variations along the transect.

3.3 Spaceborne data

The algorithms for MERIS and flow-through data are shown in Table 5. Figure 7 shows the scatter plot for chl a with MERIS data and Figure 8 shows the same for $a_{\text{CDOM}}(400)$. The values of the RMSE for each OSS with spaceborne and flow-through data are also shown in Table 5.

Figure 7 also includes data points from sources other than the spring 2004 campaign. Two of these (Validation 1) are from routinely measured stations (composite samples from 0 to 4 m depth) visited on April 27, 2004 (the same day as the spring 2004 campaign) approximately 20 km west from the campaign area. The rest (seven data points) were measured on April 25, 2005. The corresponding MERIS image was acquired on that same day at 12:27 local time. Two of these points (Validation 2) are from routine monitoring stations near Helsinki (again composite samples from 0 to 4 m depth). Five points (Validation 3) were part of a measurement campaign conducted approximately 120 km west from Helsinki (sampling depth approximately 0.2 m). The locations of these data points are shown in Figure 1. The points were used to test the validity of the chl a algorithm. The BIAS-error for these points is $5.2 \mu\text{g/l}$ and the RMSE is $10.6 \mu\text{g/l}$.

The amount of flow-through points within MERIS pixels varies from 1 to 269 (average is 45). If the MERIS pixels that contain less than 10 flow-through points are excluded the results improve slightly (R^2 increases between 0.1 and 1.8%-units depending on the OSS) and the number of data points drops to 62. The results improve significantly if the MERIS pixels that contain less than 20 flow-through points are excluded. These values are also shown in Table 5.

Figure 9 shows the thematic map for chl a with MERIS data. Airborne data are also included in the image. Figure 10 shows the same for $a_{\text{CDOM}}(400)$. Figure 11 shows the values of TSS, chl a and $a_{\text{CDOM}}(400)$ retrieved with MERIS and flow-through data as a function of the distance from the beginning of the boat transect. The data used here includes some areas that the AISA data does not cover (sampling station S4). Hence, the behavior of data in Figure 11 is different from Figure 6.

The pixels of the level 2 data that are from the campaign area (and also most of the Gulf of Finland) were all flagged as invalid. Hence, a comparison with our result was not possible. The chl *a* concentrations given in the product range between approximately 0 and 25 $\mu\text{g/l}$. These are clearly below the concentrations obtained with water sample data.

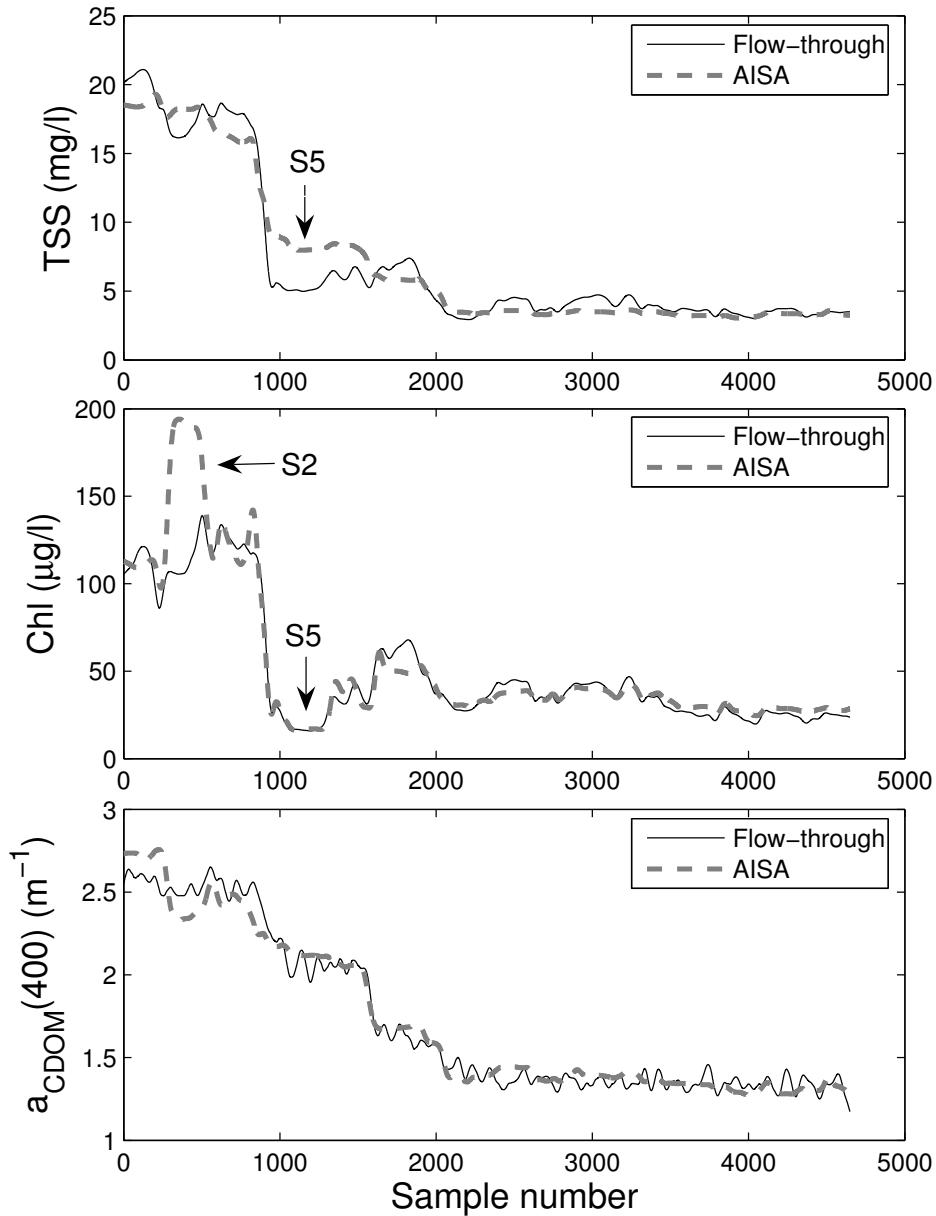


Figure 6. OSS values with flow-through and AISA data after filtering with moving average filter (span length 40 samples) as a function of distance from the beginning of the boat transect.

Table 5. Retrieval algorithms, the coefficients of determination (R^2 in %) and the root mean square errors (RMSE) for MERIS and flow-through data.

Algorithm	Chl a ($\mu\text{g/l}$)	TSS (mg/l)	$a_{\text{CDOM}}(400)$ (m^{-1})
	$275 \frac{L_{709}}{L_{665}} - 189$	$90.0 \frac{L_{709}}{L_{560} + L_{665}} - 19.6$	$8.53 \frac{L_{665}}{L_{490}} - 1.11$
R^2 for all data ($n = 73$)	81.6	88.8	95.3
R^2 (%) with some pixels excluded ^a ($n = 51$)	86.7	92.3	96.0
RMSE (% from the mean value)	7.8 $\mu\text{g/l}$ (22 %)	0.74 mg/l (16 %)	0.08 m^{-1} (5 %)

^a These results include only those MERIS pixels that contain 20 or more flow-through data points.

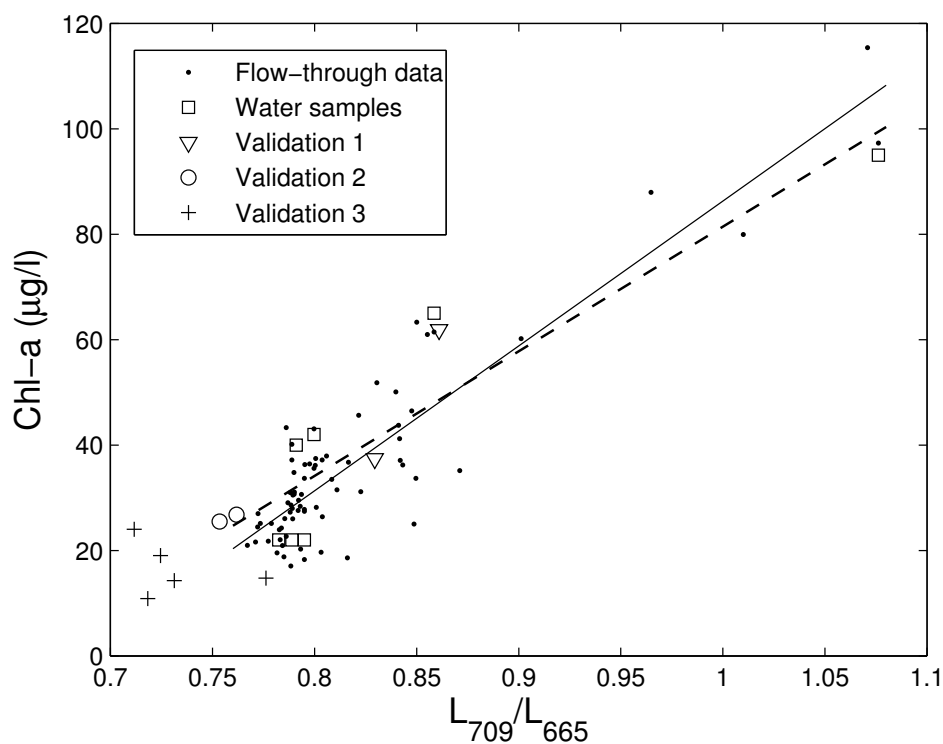


Figure 7. Chl a vs. MERIS channel ratio (L_{709}/L_{665}). The flow-through data have been preprocessed by averaging the values found within each MERIS pixel that observed at least some area of the boat transect ($n = 73$, $R^2 = 81.6\%$). For the water sample data: $n = 7$ and $R^2 = 84.3\%$. ‘Validation 1’ are data measured outside the campaign area on April 27, 2004. ‘Validation 2’ and ‘Validation 3’ are data measured on April 25, 2005. See section 3.2 for details.

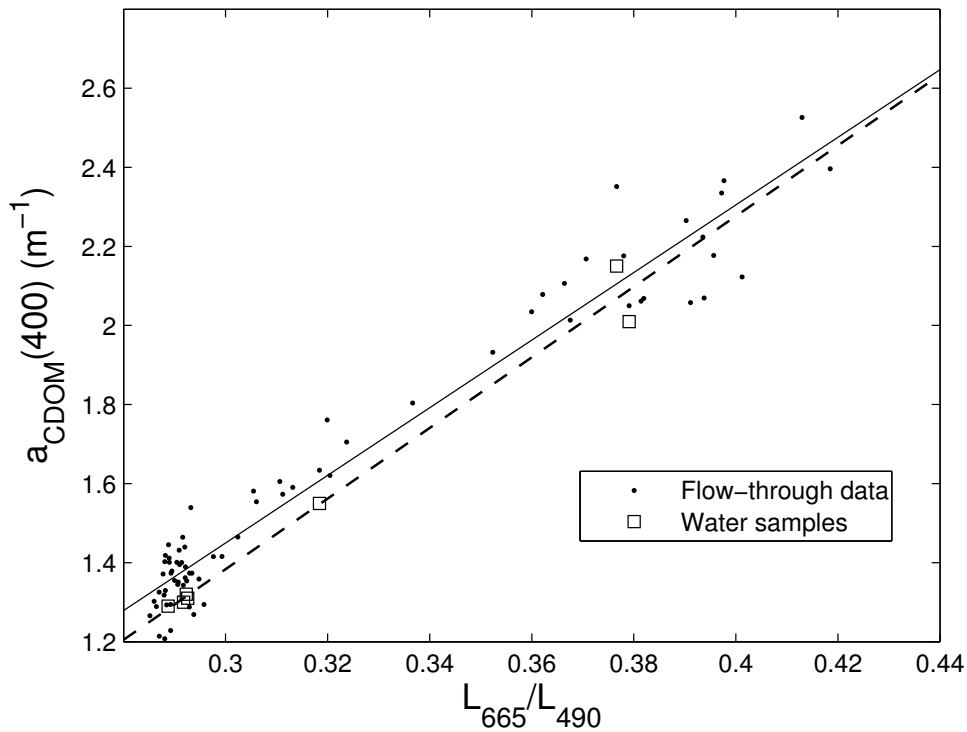


Figure 8. $a_{\text{CDOM}}(400)$ vs. MERIS channel ratio (L_{665}/L_{490}). The flow-through data have been preprocessed by averaging the values found within each MERIS pixel that observed at least some area of the boat transect ($n = 73$, $R^2 = 95.3\%$). For the water sample data: $n = 7$ and $R^2 = 98.4\%$.

3.4 Effects of atmospheric variations on MERIS estimation

The results of the procedure outlined in equations (2) to (5) are shown in Figure 12. The error for chl a and $a_{\text{CDOM}}(400)$ is below 20%. For TSS the error is almost 40% when the TSS concentration is small, but falls quickly below 20% when the concentration increases to about 6 mg/l.

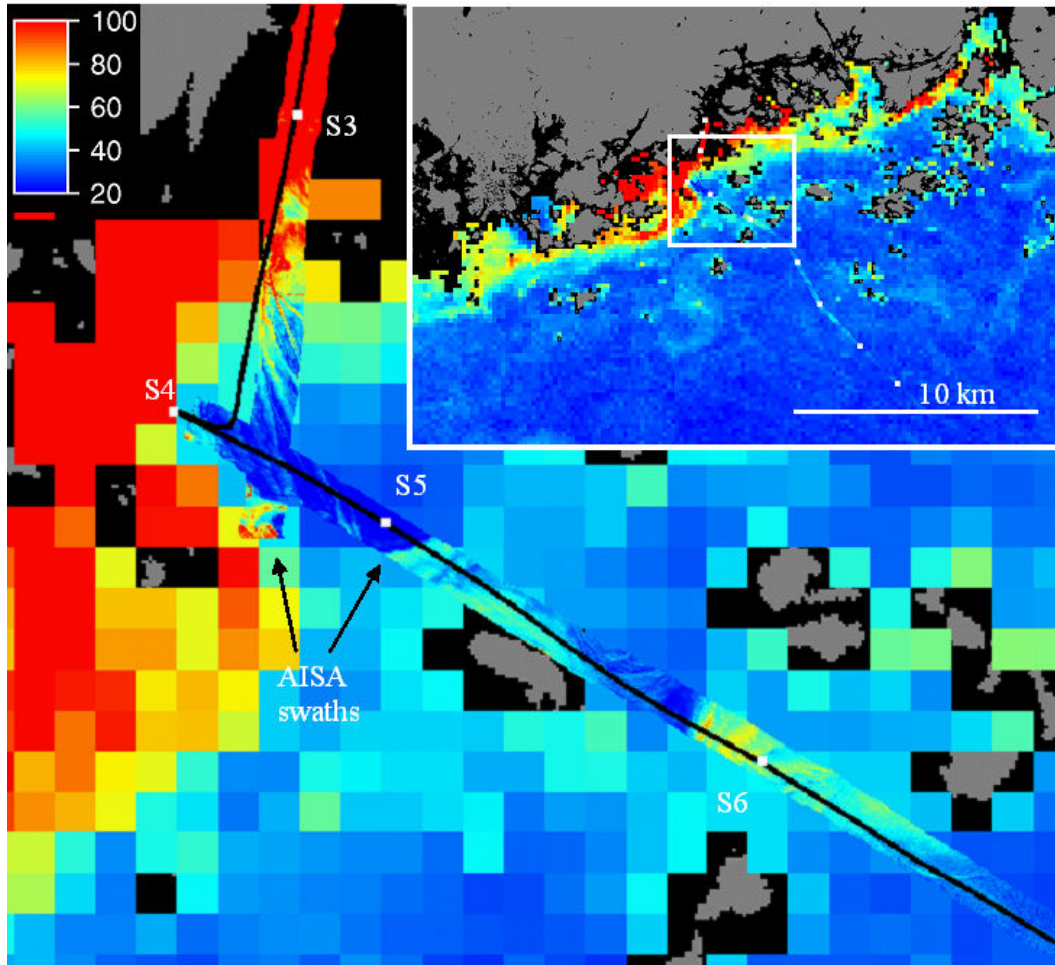


Figure 9. Chl *a* (in $\mu\text{g/l}$) with MERIS and AISA data. The concentrations over $100 \mu\text{g/l}$ are shown in red. S3-S6 are sampling stations. The small window shows an overview of the area, while the larger one shows the northern part of the airborne data where the most interesting features are present. The black curve shows the boat transect.

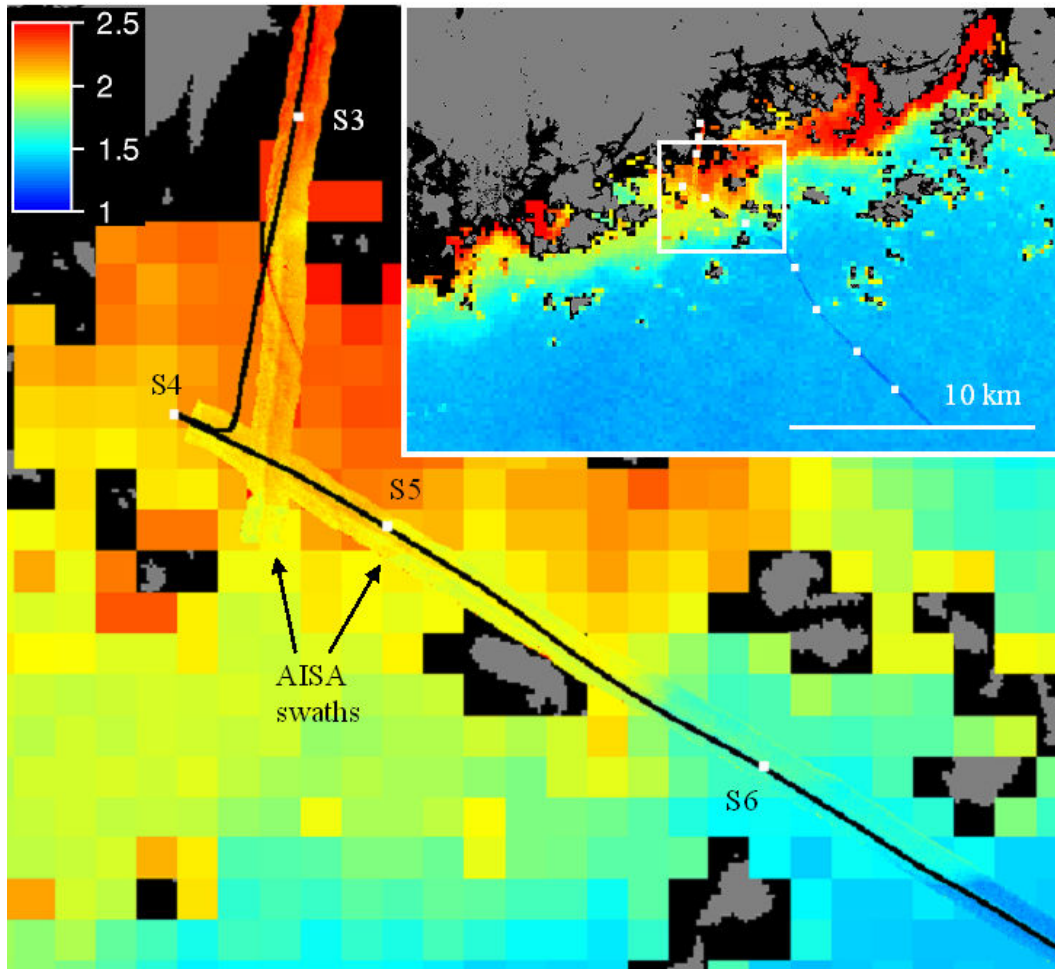


Figure 10. $a_{CDOM}(400)$ (in m^{-1}) with MERIS and AISA data. The values over $2.5 m^{-1}$ are shown in red. The black curve shows the boat transect.

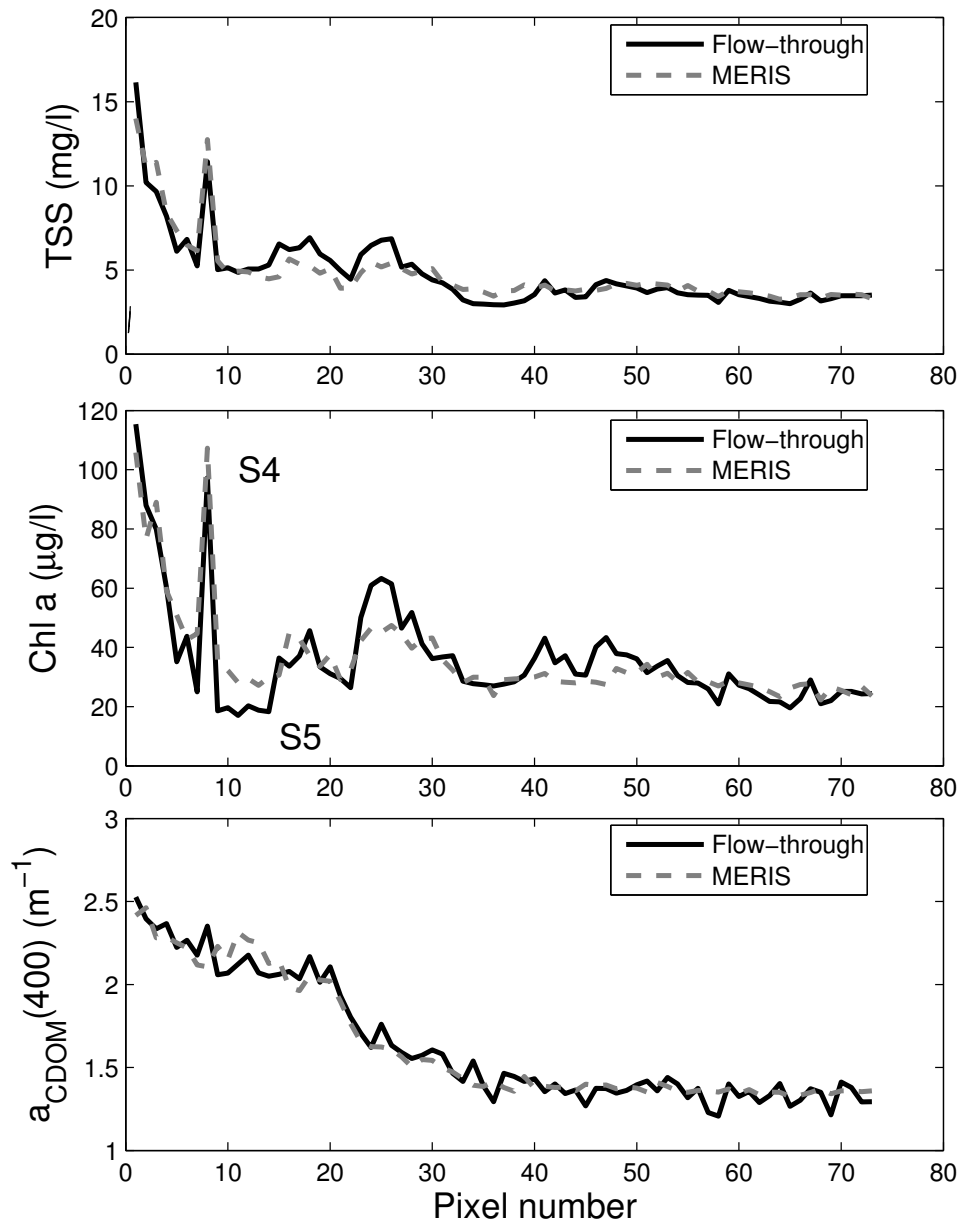


Figure 11. TSS, chl *a* and $a_{\text{CDOM}}(400)$ values with MERIS and flow-through data averaged within each MERIS pixel as a function of distance. The area covered by the data is slightly different from those presented in Figure 6 (e.g. the AISA data did not cover S4), and thus a direct comparison is not possible for all parts of the transect.

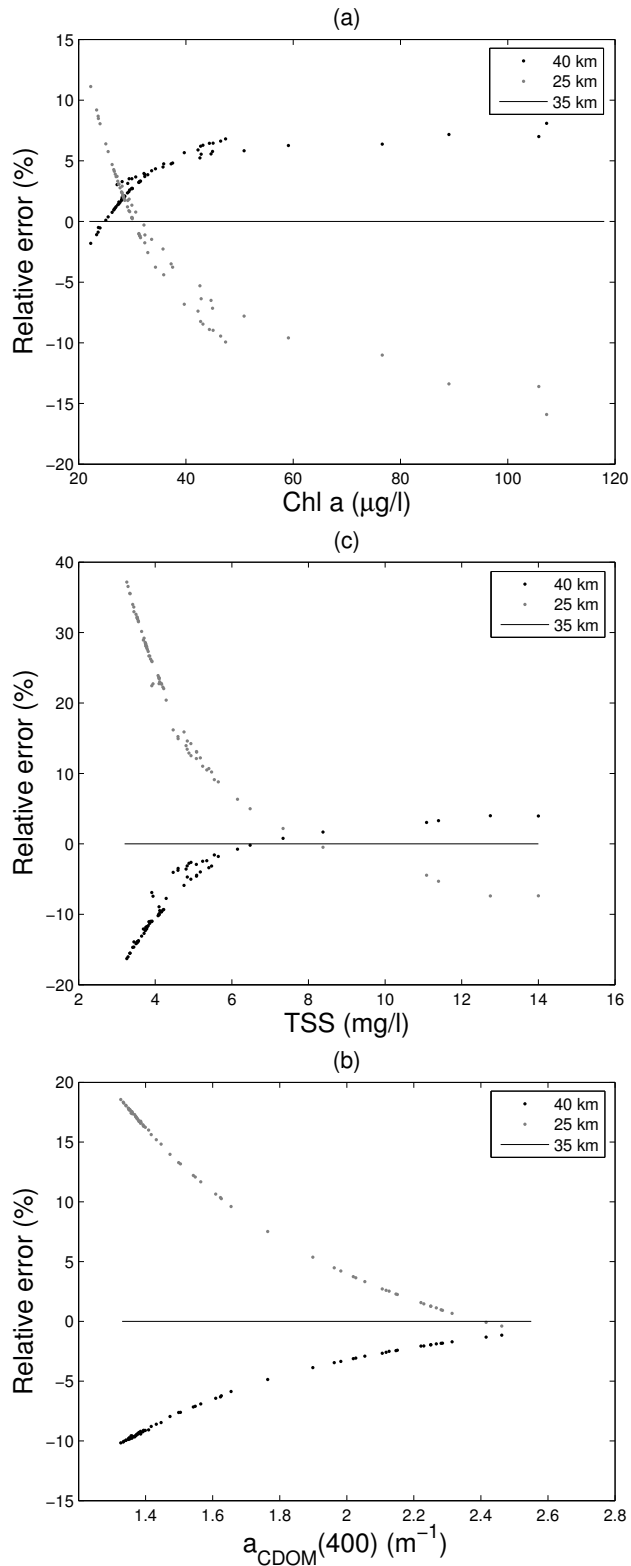


Figure 12. The relative (to the visibility = 35 km -case) errors of fixed band-ratio algorithms (see Table 5) for (a) chl a , (b) $a_{\text{CDOM}}(400)$ and (c) TSS under varying atmospheric conditions (visibility = 25 km or 40 km).

4 DISCUSSION

The values of OSS measured in a laboratory have high correlation coefficients with the airborne and spaceborne data (R^2 close to or above 0.9 in most cases). The correlations with the flow-through OSS data and remote sensing data are also high. With airborne data the coefficients of the algorithms for laboratory (Figure 3) and flow-through data (Table 4) are very close to each other. That was expected since the correlations between flow-through and laboratory data are also high.

The values of chl *a*, TSS and $a_{CDOM}(400)$ are very high at some points of the transect. This may partially explain the good results of the empirical algorithms used here as the signal from water is strong when the concentration of OSS is high. There is also some quite visible clustering around two water types with the airborne chl *a* data (Figure 5; one with chl *a* concentrations around 80-140 $\mu\text{g/l}$ and one with lower chl *a* concentrations near 20-60 $\mu\text{g/l}$). This can also lead to high R^2 values. The area observed here had a clear transition from high values to low values and the number of data points with moderate values is not very high. However, even those points do fall near the trend line of the algorithm, which improves its credibility. Spring blooms like the one observed here are not uncommon in the Gulf of Finland, and thereby, the capability of observing them accurately is important.

The validity of the chl *a* algorithm was tested using data collected outside the campaign area and on another date. As shown in the scatter plot in Figure 7 these points follow the trend-line of the algorithm quite closely. The RMSE of these points is only slightly larger than the RMSE of the data used in the calibration of the algorithm (10.6 $\mu\text{g/l}$ compared to 7.8 $\mu\text{g/l}$) and the BIAS-error is also small.

The correlations between chl *a*, TSS and $a_{CDOM}(400)$ shown in Table 3 are relatively high. The interdependence between chl *a* and TSS is quite strong. The explanation for this is that TSS contains the organic particles in addition to the inorganic ones and most of the particles present in a bloom are organic ones. The dependence between chl *a* and $a_{CDOM}(400)$ is much weaker. Despite the high correlation, there are also clear differences in the spatial behavior of the OSS. Chl *a* and TSS can have very dynamic features while the values of $a_{CDOM}(400)$ change much more gradually from high values near the coast to lower values in the open sea. The remote sensing instruments used here were able to detect this behavior, as shown in Figure 6 and Figure 11.

Filtering the data in the flow-through vs. airborne analysis improves the results. The improvement was largest for $a_{CDOM}(400)$ (R^2 increased from 92.5 to 97.1 %). The main reason for this is that the $a_{CDOM}(400)$ data from the flow-through instrument are noisy. For the flow-through vs. satellite data analysis the filtering is not necessary due to the spatial averaging caused by the 300 m pixel size. However, removing pixels that contain a low number (less than 20) of flow-through data points improves the results. This is due to the fact that the MERIS pixels cover larger areas than the flow-through data and can contain larger variations in water quality. Hence, only when MERIS pixels are sufficiently covered with flow-through data can proper analysis take place. This is a problem also for the water sample data since each sample only covers a single point in the MERIS pixel. Kutser (2004) demonstrates similar problems by analyzing the spatial distribution of chl-*a* concentrations retrieved with high resolution satellite instruments in the Gulf of Finland during a cyanobacterial bloom.

The measured chl-*a* concentrations are quite low near S5 when compared to the rest of the coastal area. This applies to both laboratory and flow-through data as well as for airborne data. The low concentrations are also visible in the MERIS image, although the magnitude of the change is not as clear. The values of TSS and $a_{CDOM}(400)$ also change but not as dramatically. Also, the AISA spectrum (Figure 2) has an interesting behavior at S5. The reflectance is quite high at 550 nm (at same levels as at S1-S3) but then drops quickly to the same levels as S8, S9 and S10 have as the wavelength increases. The algorithms based on channel ratios are able to compensate for the behavior of the spectra (i.e. the data point is not an outlier). The TSS algorithm for airborne data, which is based on one channel only, is not.

The spatial changes in the satellite data are much less dynamic. This is due to the larger pixel size – the spatial changes are averaged out as the pixel size increases. However, the smaller scale changes in the OSS values can still be observed with satellite data in addition to the overall change from high values near the coast to lower values in the open sea.

The spatial variability of AISA data versus the flow-through measurements of this same campaign was investigated in Pyh alahti et al. (2004). As spatial averaging was applied to these measurements, the properties of optimal algorithms for interpreting the spectrometer data into observed water quality changed. According to the observed spatial correlation characteristics, the changes were most pronounced in the resolutions in the order of or higher than those of the MERIS instrument. The results encourage the use of flow-through measurements in satellite vs. *in situ* data analysis instead of point sampling, as demonstrated in Lindfors et al. (2005).

One possible reason for the differences between *in situ* observations and remote sensing data is that the water samples and the flow-through data are collected from 0.5 m below surface, while remote sensing instruments observe, especially in turbid waters, the topmost surface layer of water. Since the values of OSS are quite high, the penetration depth of light into water is low (Secchi depth was 0.6 m at S1 and S3).

The time difference between *in situ* observations and remote sensing data acquisition, even though being relatively small, can also affect the results when high-resolution data from airborne instruments such as AISA are used. Here, the time difference between the airborne data and flow-through data is about one hour at the starting point of the transect. Depending on wind speed and direction, and local currents it is possible that water moves during the time difference and the area measured with the remote sensing instruments is not the same as the area sampled with *in situ* observations.

The coefficients of the algorithms presented in Table 4 (airborne data) are different from those presented in Table 5 (MERIS data). The reason for this is that the MERIS data are influenced by the whole atmosphere while the airborne data are influenced by what is below its 1 km flight altitude. The coefficients are valid only for the two cases analyzed here. If another dataset is obtained the algorithms have to be trained again with *in situ* observations. However, those are not always available so retraining may not be possible. Fortunately, the amount of error caused by not retraining the algorithm can be estimated. According to the MODTRAN simulations, the error due to changes in the atmospheric conditions for the chl *a* and $a_{CDOM}(400)$ estimation is less than 20 % in most cases as a prefixed band-ratio algorithm according to Table 5 is employed. For TSS the error is larger. The errors are also larger in the low end of TSS and $a_{CDOM}(400)$

values. One reason for this is that since the signal with low OSS values is weak the noise from the atmosphere is able to disturb the estimation more. Another reason is that the error is shown as a function of the OSS, so even if the absolute error would be a constant, the relative error would be larger with low OSS.

The error for $a_{CDOM}(400)$ is in most cases larger than for chl *a*. In the $a_{CDOM}(400)$ algorithm the channels are in different parts of the spectrum (one in the blue and one in the red region) while in the chl-*a* algorithm the channels are close to each other (one in the red region and the other close to it in the NIR region). When the atmospheric conditions change, the values of T_{atm} and L_{atm} change more in the blue region than in red or NIR. Hence, an algorithm based on a red/blue ratio is more susceptible for atmospheric changes than a NIR/red –algorithm. Similar results for chl *a* were also found in Attila et al. (2006) where simulated AISA data were used with the same MERIS channel combination. The small errors in chl-*a* algorithm can be related to the relatively high chl-*a* concentrations in the dataset. The lowest chl-*a* concentration was 22 $\mu\text{g/l}$.

As the estimation of OSS in this work is based on empirical relationships the algorithms may also (in addition to atmospheric effects) require retraining if the specific inherent optical properties (SIOP) of water differ from those studied here (e.g. if the species composition of the phytoplankton changes). In Kallio et al. (2001), concurrent AISA and water quality data were collected from 11 lakes in southern Finland on eight days between August 1996 and August 1998. One of the measurement days was in May (dominated by diatoms) while the others were in August (dominated by cyanobacteria). The estimation algorithms were developed separately for May and August data and the resulting slope and the intercept values were found to be slightly season specific. Thus, the algorithms presented in this work should be calibrated with *in situ* data if they are to be used with remote sensing observation from the late summer or fall season.

The wavelengths of the algorithm in Kallio et al. (2001) were slightly different from the ones used in this study, so the comparison of regression coefficients was not possible.

Analytical methods based on bio-optical models can be used for water quality estimation with remote sensing data instead of empirical band-ratios. Analytical methods have the advantage of being based on the basic interactions (scattering and absorption) between OSS and radiation and thus are generally more valid for different areas and water types. However, the bio-optical models for this area are still under development. One version has been parameterized with chl *a* values that are below 72 $\mu\text{g/l}$ (Kallio et al. 2005, Kallio 2006). This is clearly below the values present in the spring bloom data. Also, the problem of defining the Q and f-factors for analytical algorithms remains. Both Q and f are functions of the measurement angle and the inherent optical properties (IOP) of water (and hence the concentrations of chl *a*, TSS and CDOM). The published values for Q and f are limited to low chl-*a* concentrations (e.g. 0.3 $\mu\text{g/l}$ to 10 $\mu\text{g/l}$ in Morel et al. (2002) for Case 1 waters). Hence, the analytical methods need more work before they can be applied to water with high concentrations of chl *a* and other optically significant substances. The empirical method used here on the other hand worked well with the extreme concentrations present in a spring bloom.

It should also be noted that while empirical methods require concurrent *in situ* data for training or calibration they generally work very well if such data are available. In the Baltic Sea the availability of *in situ* data has improved due to, for example, the growing

number of flow-through devices operating in the region (e.g. Alg@line: Rantajarvi 2003).

The MERIS FR level 2 ocean product data (from the same date and time as the level 1b data used in our analysis) were flagged as invalid over the measurement area and also most of the Gulf of Finland. Hence, it was not possible to compare our results with the standard MERIS retrieval procedures used by ESA. The likely reason for the failure of the standard product is that the water in the Baltic Sea in general and in this case in particular, is more turbid and contains more chl *a*, TSS and CDOM than the waters used in the development of the standard MERIS algorithm. The neural network, which is used in the standard processing, has been trained to resolve OSS properties for a certain range of OSS values. Some of the areas observed in this case study (the ones closest to the shore) have OSS values that are clearly outside these ranges and thus outside the area of applicability of this particular neural network algorithm. In these areas the official MERIS processing system is performing quite correctly, as it flags these pixels invalid. However, high OSS values, such as the ones presented here, are regularly observed in the Gulf of Finland during the spring bloom season and one purpose of the analysis described in this paper is to explore the possibilities of OSS detection beyond the range of applicability of the current standard ESA processing methods.

5 CONCLUSIONS

The objective here was to investigate the feasibility of using MERIS for estimating water quality in an area where the coastline is fragmented and the spatial variation of the water quality is large. The retrieval of chl *a*, TSS and CDOM was successful even though the standard MERIS processing failed to provide reliable data. The accuracy of the estimation (R^2) for each OSS was close to or above 0.9. The results indicate that a satellite sensor with characteristics similar to MERIS is suitable for remote sensing of water quality in fragmented coastal regions. However, the retrieval algorithms still need to be refined. The results with the MODTRAN simulation indicate that band-ratio algorithms developed with a dataset from a single occasion are relatively insensitive to atmospheric variations.

The accuracy of the estimation with airborne data was above 0.9 for all OSS. The behavior of airborne data as a function of distance (Figure 6) is similar to the behavior of MERIS data (Figure 11). This indicates that MERIS is capable of retrieving OSS values that are similar to the data provided by higher resolution instruments although some spatial variation is lost due to larger pixel size.

ACKNOWLEDGEMENTS:

The Envisat MERIS data was provided by the European Space Agency.

Appendix I: Estimation of $a_{\text{cdom}}(400)$ from ac-9 data.

For the estimation of $a_{\text{cdom}}(400)$ we first calculated $a_{\text{cdom}}(412)^*$ from ac-9 data by subtracting absorption coefficient of phytoplankton from the measured $a(412)$:

$$a_{\text{cdom}}(412)^* = a(412) - 1.43 \cdot a(676),$$

where $a(412)$ and $a(676)$ are absorption coefficients at 412 and 676 nm measured with ac-9 (with pure water absorption subtracted), respectively. The asterisk denotes for the ac-9 based estimate. The coefficient 1.43 is the ratio $a_{\text{ph}}(412)/a_{\text{ph}}(676)$ (ph is for phytoplankton) obtained from the particle absorption measurements carried out in the Gulf of Finland in spring 2000 (J. Seppälä, unpublished data).

$a_{\text{cdom}}(400)^*$ was calculated from $a_{\text{cdom}}(412)^*$ by assuming an exponential increase with a decreasing wavelength and a slope factor of 0.018 nm^{-1} :

$$a_{\text{cdom}}(400)^* = a_{\text{cdom}}(412)^* \cdot e^{-0.018 \cdot (400-412)}.$$

After comparison of $a_{\text{cdom}}(400)^*$ with the $a_{\text{cdom}}(400)$ measured in laboratory $a_{\text{cdom}}(400)^*$ was additionally corrected by:

$$a_{\text{cdom}}(400) = 0.763 \cdot a_{\text{cdom}}(400)^* + 0.47, R^2 = 0.954.$$

This correction was probably due to the inaccuracy in the estimation of a_{ph} . In addition, absorption by detritus was not taken into account.

REFERENCES

- Attila J., Pyhälähti T., Hannonen T., Kallio K., Pulliainen J., Koponen S., Härmä P., Eloheimo K., 2006. Analysis of turbid water quality using airborne spectrometer data with a numerical weather prediction model-aided atmospheric correction, Photogrammetric Engineering and Remote Sensing, In press.
- Berk, A., Bernstein, L. S., & Robertson, D. C. 1989. MODTRAN: a moderate resolution model for LOWTRAN7, GLTR-89-0122, Air Force Geophys. Lab., Hanscom AFB, MA, 38 pp.
- Brockmann C., Krämer U., Stelzer K., Fournier-Sicre V., Huot J.P., Bélanger S., Fell F., Moore G., Albert P., Pinty B., Antoine D., Ramon D., Doerffer R., and Zagolsky F. (2002), Verification of the MERIS level 2 products. Envisat Validation Workshop, 9-13 December, ESRIN, Frascati, Italy.
- Carlund T., Håkansson B., Land P., 2005. Aerosol optical depth over the Baltic Sea derived from AERONET and SeaWiFS measurements. *International Journal of Remote Sensing*, 26(2), 233-245.
- Darecki M., Stramski D., 2004. An evaluation of MODIS and SeaWiFS bio-optical algorithms in the Baltic Sea. *Remote Sensing of Environment*, 89, 326-350.
- Dekker A.G., 1993. Detection of Optical Water Parameters for Eutrophic Lakes by High Resolution Remote Sensing. PhD. Dissertation, Free University, Amsterdam.
- Doerffer, R., Sorensen, K., Aiken, J., 1999. MERIS: Potential for Coastal Zone Applications. *International Journal of Remote Sensing*, 20, 1809-18.
- EN 872, 1996. Water Analysis - Determination of suspended solids. European Committee for Standardization.
- Gitelson A, Garbuzov G, Szilagyi F, Mittenzwey K-H, Karnieli, K, Kaiser A., 1993. Quantitative remote sensing methods for real-time monitoring of inland waters quality. *International Journal of Remote Sensing*, 14, 1269-1295.
- Härmä P., Vepsäläinen J., Hannonen T., Pyhälähti T., Kämäri J., Kallio, K., Eloheimo K., Koponen S., 2001. Detection of water quality using simulated satellite data and semi-empirical algorithms in Finland. *The Science of Total Environment*, 268 (1-3), 107-121.
- ISO 10260, 1992. Water quality—Measurement of biochemical parameters—Spectrometric determination of the chlorophyll-a concentration. International Organization for Standardization.
- Kallio, K., Kutser, T., Hannonen, T., Koponen, S., Pulliainen, J., Vepsäläinen, J., and Pyhälähti, T. 2001. Retrieval of water quality variables from airborne spectrometer in various lake types at different seasons. *The Science of the Total Environment*, Vol. 268, Nos. 1-3, pp. 59-78.
- Kallio, K., Koponen, S., and Pulliainen, J., 2003. Spatial distribution of chlorophyll *a* in two meso-eutrophic lakes as estimated by airborne imaging spectrometry. *International Journal of Remote Sensing*, 24 (19), 3771–3790.
- Kallio, K., Pulliainen, J. and Ylöstalo, P., 2005. MERIS, MODIS and ETM channel configurations in the estimation of lake water quality from subsurface reflectance with

- semi-analytical and empirical algorithms. *Geophysica* 41(1-2), 31-55.
- Kallio, K., 2006. Optical properties of Finnish lakes estimated with simple bio-optical models and water quality monitoring data. *Nordic Hydrology* 37(2), 183–204.
- Koponen, S., Pulliainen, J., Servomaa, H., Zhang, Y., Hallikainen, M., Kallio, K., Eloheimo, K., and Hannonen, T., 2001. Analysis on the feasibility of multi-source remote sensing observations for chl-*a* monitoring. *The Science of the Total Environment*, 268 (1-3), 95-106.
- Koponen, S., Pulliainen, J., Kallio, K., and Hallikainen, M., 2002. Lake water quality classification with airborne hyperspectral spectrometer and simulated MERIS-data. *Remote Sensing of Environment*, 79 (1), 51-59.
- Kowalczyk P., Olszewski J., Darecki M., Kaczmarek S., 2005. Empirical relationships between coloured dissolved organic matter (CDOM) absorption and apparent optical properties in the Baltic Sea waters. *International Journal of Remote Sensing*, 26(2), 345-370.
- Kutser, T., 2004. Quantitative detection of chlorophyll in cyanobacterial blooms by satellite remote sensing. *Limnology and Oceanography*, 49(6), 2179–2189.
- Lindfors, A., Rasmus K., Strömbeck N., 2005. Point or pointless – quality of ground data. *International Journal of Remote Sensing*, 26(2), 415-423.
- Morel, A. and Prieur, L., 1977. Analysis of variations in ocean color. *Limnology and Oceanography*, 22, 709-722.
- Morel, A., Antoine, D., and Gentili, B., 2002, Bidirectional reflectance of oceanic waters: accounting for Raman emission and varying particle scattering phase function. *Applied Optics*, 41(30), 6289-6306.
- Pierson, D.C. and Strömbeck, N., 2000. A modelling approach to evaluate preliminary remote sensing algorithms: Use of water quality data from Swedish Great Lakes. *Geophysica*, 36, 177-202.
- Pyhälähti, T., Vepsäläinen, J., Kallio, K., Pulliainen, J., Koponen, S., Lindfors, A., Rasmus, K., 2004. Spatial Variability of Coastal Water Quality and Its Influence on Measurements With Low and Medium Resolution Satellite Instruments. *Ocean Optics XVII*, October 2004, Fremantle, Australia.
- Rantajärvi, E., (Editor), 2003. Alg@line in 2003: 10 Years of Innovative Plankton Monitoring and Research and Operational Information Service in the Baltic Sea. Report Series of the Finnish Institute of Marine Research No. 48, 36 p.
- Rast, M., Bézy, J., and Bruzzi, S., 1999. The ESA Medium Resolution Imaging Spectrometer MERIS – a review of the instrument and its mission. *International Journal of Remote Sensing*, 20 (9), 1681-1702.
- Ruddick K., Gons H., Rijkeboer M., Tilstone G., 2001. Optical remote sensing of chlorophyll a in case 2 waters by use of an adaptive two-band algorithm with optimal error properties, *Applied Optics*, 40(21), 3575-3585.
- Ruddick K., Park Y., Nechad B., 2004. MERIS imagery of Belgian coastal waters: mapping of Suspended particulated matter and chlorophyll-a. *Proceedings of MERIS User workshop, Frascati, Italy (ESA SP-549, May 2004)*.

Schiller, H., and Doerffer, R., 1999. Neural networks for emulation of an inverse model – operational derivation of case II water properties from MERIS data. *International Journal of Remote Sensing*, 20, 1735–1746.

Siegel H., Gerth M., Ohde T., Heene T., 2005. Ocean colour remote sensing relevant water constituents and optical properties of the Baltic Sea. *International Journal of Remote Sensing*, 26(2), 315-330.

Specim, 2005. Web-page: <http://www.specim.fi>.